ACADEMIC PRESS

Available online at www.sciencedirect.com
SCIENCE DIRECT®

Journal of Catalysis 217 (2003) 284–291

JOURNAL OF CATALYSIS

www.elsevier.com/locate/jcat

Kinetics of the hydrodenitrogenation of *o*-toluidine over fluorinated $NiMoS/Al_2O_3$ and NiMoS/ASA catalysts

Lianglong Qu, Martin Flechsenhar, and Roel Prins *

Laboratory for Technical Chemistry, Federal Institute of Technology, ETH-Hönggerberg, 8093 Zurich, Switzerland

Received 12 August 2002; revised 24 October 2002; accepted 18 November 2002

Abstract

The kinetics of the hydrodenitrogenation of *o*-toluidine has been studied between 330 and 370 °C at 5.0 MPa in a continuous microflow reactor over sulfided and fluorinated NiMo catalysts supported on alumina as well as silica–alumina. The silica–alumina-supported catalysts exhibited a higher hydrodenitrogenation activity than their alumina-supported counterparts. In situ fluorination promoted the hydrodenitrogenation activity by mainly enhancing the activity for the saturation of the aromatic ring. Kinetic parameters for the reaction network were obtained by fitting the experimental results with Langmuir–Hinshelwood equations. The reaction rate constants of the alumina- as well as silica–alumina-supported NiMo catalysts increase substantially after fluorination. The activation energies and the heats of adsorption are about the same over all catalysts. This indicates that the intrinsic activity of the active sites is not influenced by the in situ fluorination and by the support; only the number of hydrodenitrogenation sites is increased by a higher stacking of MoS_2.

Keywords: HDN; Hydrodenitrogenation; Kinetics; *o*-Toluidine; Methylcyclohexylamine; NiMo catalysts; In situ fluorination; Alumina; Silica–alumina

1. Introduction

Hydrodenitrogenation (HDN) is one of the key processes in oil refining. Its main purpose is to eliminate nitrogen from engine fuels and petroleum distillates in order to minimize NO_x emission upon burning and to prevent downstream acidic catalysts from poisoning. With the increasing demands for upgrading heavy feed stocks, coal-derived liquids, and oil shale, as well as more stringent environmental regulations, better knowledge of HDN is needed to develop new catalysts and processes for the efficient removal of nitrogen [1]. *o*-Toluidine is a convenient nitrogen-containing model compound to study the mechanism and kinetics of HDN [2,3]. The HDN of toluidine mainly takes place via hydrogenation to methylcyclohexylamine (MCHA). This MCHA then reacts to methylcyclohexene (MCHE) and methylcyclohexane (MCH) (Fig. 1). Only traces of MCHA are detected as primary reaction intermediates in the HDN of toluidine because its rate of formation is much slower than its rate of further reaction. Nevertheless, MCHA may have a strong inhibition effect on the HDN of toluidine. This complicates the kinetic modeling of the HDN network of toluidine and makes it difficult to obtain reliable kinetic parameters. Therefore, we have studied separately the HDN of MCHA [4] and the reaction of olefin hydrogenation [5]. In this paper, we will describe the kinetics of the HDN of *o*-toluidine (*o*-methylaniline, OMA).

Fluorine is widely used in hydrotreating catalysts. Several studies have furthered the understanding of the effect of fluorine in hydrotreating catalysts [6–20], but only a few dealt with HDN [7,8,10,11]. The enhancement of the HDN activity by fluorine addition has been assigned to the higher acidity of fluorine-containing catalysts, the better dispersion of the metals on the fluorine-modified supports, as well as the higher chemisorption capacity for hydrogen. In most cases, fluorination is performed by impregnating the support with a fluoride salt, like NH_4F (see, e.g., Refs. [6,13]). After NH_4F impregnation, drying, and calcination, molybdenum and nickel are introduced as usual by impregnation. After a subsequent calcination, the resulting materials are sulfided in a stream of H_2S in H_2. Thus, in this method the dispersion of the resulting MoS_2 and Ni sulfides may be different in the fluorine-containing and fluorine-free NiMo catalysts, caused by the different surface properties of these supports. Conclusions about the effect of fluorine are then difficult

* Corresponding author.
E-mail address: prins@tech.chem.ethz.ch (R. Prins).

0021-9517/03/$ – see front matter
doi:10.1016/S0021-9517(02)00174-4

to make. In situ fluorination, after preparation of the NiMo catalysts in their sulfidic form, has been described in patents (see, e.g., Refs. [21,22]), but not in the open literature. Because in this method the metal sulfides are prepared before fluorination, the surface properties of the support will not influence the catalyst dispersion. This might allow one to draw firm conclusions about the real chemical effect of fluorine in HDN, apart from any change in dispersion.

Amorphous silica–alumina (ASA) seems to be a promising support in hydroprocessing. Many studies and patents have described its use in aromatics hydrogenation [23–25], mild hydrocracking [26], hydrocracking [25,27–29], HDS [24,25,29–35], and HDN [29,36] using noble metal-based [23–25,27,28,30,32,35,36] and Mo- and W-based catalysts [26,29,31,33–35]. Better performances were reported for ASA-supported catalysts than for their conventional Al_2O_3-supported counterparts. Only a few studies dealt with HDN over Mo- and W-based catalysts. In previous studies over supported NiMo catalysts, we already described that the ASA support substantially increased the activity for the HDN of MCHA [4] and lowered the rate of hydrogenation of olefins [5]. The in situ fluorination had a promoting effect on the HDN of MCHA and no effect on the hydrogenation of cyclohexene. In this paper, the kinetics of the HDN of OMA was studied over sulfided and fluorinated NiMo catalysts supported on Al_2O_3 and ASA. By comparing the kinetic parameters, the effects of in situ fluorination and of the support on the HDN of the aromatic nitrogen-containing compound could be studied.

2. Experimental

Catalysts containing 4 wt% Ni and 13 wt% Mo supported on γ-Al_2O_3 (Condea) and amorphous silica–alumina (prepared by the sol–gel method, containing 25 wt% Al_2O_3) were prepared by sequential pore volume impregnation with aqueous solutions of ammonium molybdate tetrahydrate (Fluka) and nickel nitrate hexahydrate (Fluka) with Mo first, followed by drying overnight at 120 °C and calcining at 500 °C in air after each impregnation step. The $NiMo/Al_2O_3$ catalyst had a pore volume of 0.42 ml g^{-1} and a surface area of 155 $m^2\,g^{-1}$ as measured by BET nitrogen adsorption. The NiMo/ASA catalyst had a pore volume of 0.43 ml g^{-1} and a surface area of 265 $m^2\,g^{-1}$. The HDN reaction was carried out over 0.05 g (in situ fluorinated) of a sulfided $NiMo/Al_2O_3$ or NiMo/ASA catalyst diluted with 8 g SiC to achieve plug–flow conditions in a high-pressure microreactor. The catalyst was first dried for 2 h at 400 °C and then sulfided with a mixture of 10% H_2S in H_2 at 1.0 MPa. Sulfidation started from ambient temperature with a slow temperature increase in 14 h to 370 °C and temperature was then maintained for 2 h. In situ fluorination was performed with a solution of *o*-fluorotoluene in octane at 370 °C while continuing the sulfidation [5,10]. The pressure was first increased to that of the reaction condition (5.0 MPa) with the sulfiding gas. After cooling the reactor to 200 °C, a solution of 0.26 wt% *o*-fluorotoluene (Fluka) in *n*-decane (Fluka) was dosed to the reactor with a syringe pump (Isco 100D). The temperature was slowly raised to 370 °C and kept for 48 h, while the sulfiding and fluorination gas was flowing through the reactor. The fluorine contents in the thus fluorinated catalysts were about 1 wt% determined by X-ray fluorescence absorption. The total amount of fluorine passed over the catalyst was 6% on the basis of catalyst weight. Because the retained F content was only 1%, the conversion of *o*-fluorotoluene to HF and toluene was low. As a consequence, and because we used a microreactor containing only 50 mg catalyst, there will be no F gradient over the catalyst bed.

After activation, the pressure was kept at 5.0 MPa and the temperature at 370 °C. A solution of *o*-toluidine and cyclohexene (CHE) in octane (with *n*-heptane as the internal standard and dimethyldisulfide to generate H_2S in situ) was fed to the reactor. Partial pressures at the reactor inlet were $p_{OMA} = 2$, 7, 10, or 14 kPa, $p_{CHE} = 4$ kPa, $p_{H_2S} = 17.5$ kPa, $P_{H_2} = 4.8$ MPa, and octane was the balance.

The reaction products were analyzed by on-line gas chromatography (Varian Star 3400CX equipped with a 30-m DB-5MS fused silica capillary column and a flame ionization detector). All kinetic data were obtained by varying the weight time and reactant initial partial pressure after stabilization for 20 h. Weight time was defined as the catalyst weight divided by the total molar flow fed to the reactor. The hydrogen flow rates were always changed in proportion to the liquid flow rates. No diffusion and transport limitations were detected from conversion of OMA under the conditions studied. This allowed us to model the reaction with a Langmuir–Hinshelwood mechanism assuming adsorption equilibrium for the HDN compounds. The program we used for the nonlinear numeric fitting was the SCIENTIST by MicroMath Inc.

3. Results and discussion

3.1. HDN reaction scheme of OMA

The HDN network of OMA is shown in Fig. 1. There are two reaction pathways in the HDN of OMA over (fluorinated) sulfided $NiMo/Al_2O_3$ and NiMo/ASA catalysts: path 1 is the hydrogenation of OMA to MCHA, with further reaction to MCHE and MCH, and path 2 the direct hydrogenolysis of OMA to toluene. The formation of MCHE and MCH from OMA can be attributed to the hydrogenation of the phenyl ring to MCHA, followed by breaking of the $C(sp^3)$–N bond by elimination of NH_3 and hydrogenation of the resulting MCHE to MCH. There is also a direct path from MCHA to MCH [2,3]. A small amount of ethylcyclopentane (ECP) is formed by isomerization of MCHE and subsequent hydrogenation. The formation of toluene indi-

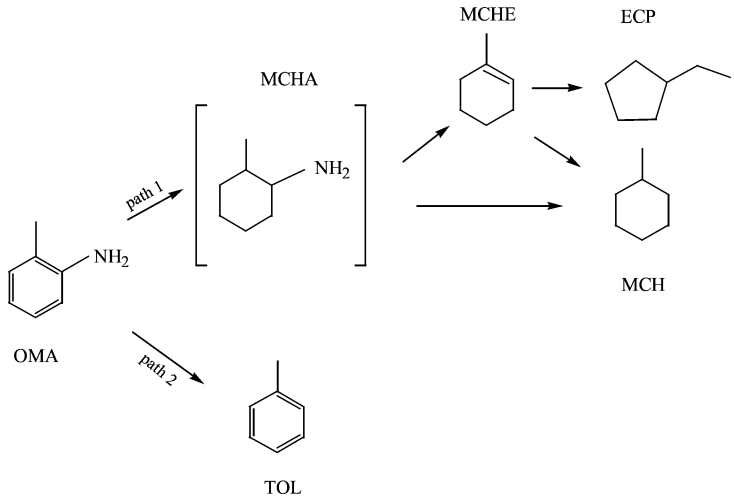

Fig. 1. Reaction network for the HDN of OMA over $NiMo/Al_2O_3$ and NiMo/ASA catalysts.

cates that a direct $C(sp^2)$–N bond cleavage occurred, which accounted for about 10% of the total conversion.

The product distribution versus weight time plot clearly shows that MCHE is an intermediate and MCH the final product (Fig. 2). MCHE is formed at a relatively high concentration as long as the OMA concentration is reasonably high. This is similar to what happens during the HDN of MCHA [4], which indicates that a strong (competitive adsorption) inhibition of OMA and MCHA on the hydrogenation of MCHE takes place. This is also evident from a comparison of the CHE conversion obtained with a pure CHE feed at 350 °C with that obtained with a mixed feed of CHE with either 14 kPa of OMA or 14 kPa of MCHA (Fig. 3). Obviously, both OMA and MCHA substantially inhibit the hydrogenation of CHE, but MCHA is a stronger inhibitor than OMA.

No MCHA was observed under our conditions in the HDN of OMA, due to the fast reaction of MCHA to MCHE and NH_3. The MCHA intermediate reacts faster away than it diffuses out of the catalyst pores and is not detected at the exit of the reactor [3]. Nevertheless, we cannot exclude that the (low) concentration of MCHA in the pores of the catalyst has an inhibition effect on the HDN of OMA and on the hydrogenation of MCHE and CHE. MCHA could be detected in the HDN of OMA when a large amount of CHE was added to the reaction mixture [3]. Direct proof of the inhibition effect of MCHA on the HDN of OMA was that, in the presence of 14 kPa MCHA, the HDN of OMA was strongly inhibited (Fig. 4). Only after most of the MCHA had reacted away, did the HDN of OMA start. No increase in the formation of ECP was observed with NiMo/ASA and fluorinated catalysts compared to $NiMo/Al_2O_3$. When OMA or MCHA was present in the reaction mixture, no isomerization of CHE to methylcyclopentane (MCP) occurred.

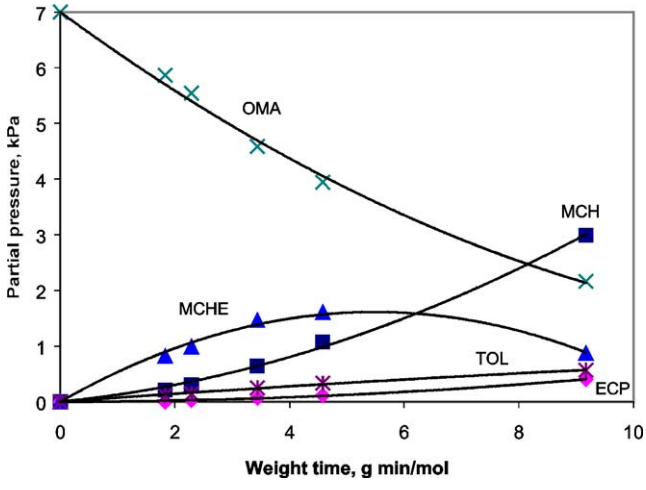

Fig. 2. Product distribution during the HDN of 7 kPa OMA at 370 °C over F-NiMo/ASA.

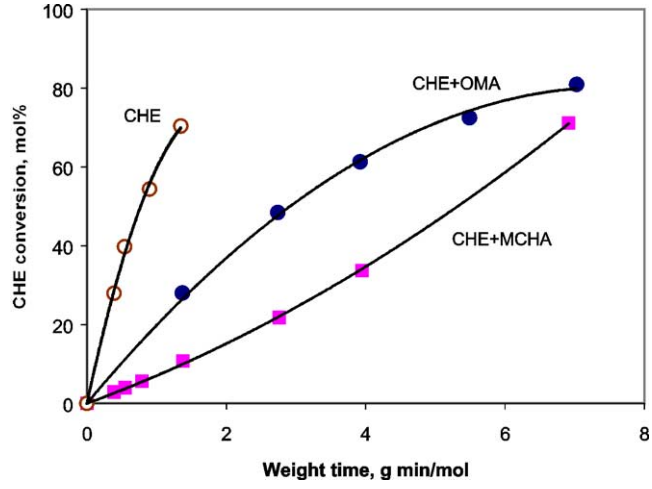

Fig. 3. Inhibition of 14 kPa OMA and MCHA on the hydrogenation of 4 kPa CHE at 350 °C over $NiMo/Al_2O_3$ expressed by CHE conversion versus weight time.

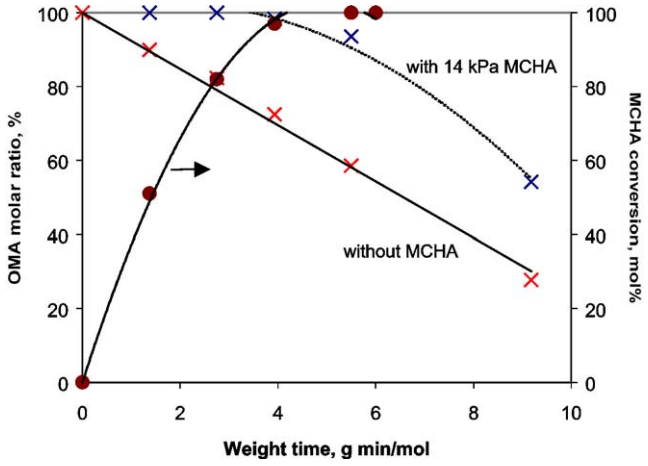

Fig. 4. Inhibition of 14 kPa MCHA on the HDN of 7 kPa OMA at 350 °C over NiMo/ASA.

3.2. Support effect

From the conversion of OMA and CHE on the NiMo catalysts supported on Al_2O_3 and ASA (Fig. 5), it is clear that both the fluorine-free and the fluorine-containing ASA-supported catalysts have a higher HDN activity and a lower olefin hydrogenation activity than their Al_2O_3-supported counterparts. The higher activity for the hydrogenation of olefins over Al_2O_3-supported catalysts has been attributed to the higher dispersion of MoS_2 on the Al_2O_3 support [5]. More MCHE and less MCH is produced over the ASA-supported catalyst than over the Al_2O_3-supported catalyst (Fig. 6). This holds for the fluorinated catalysts as well (not shown here). The effect of the support on the selectivity of MCHE and MCH during the HDN of OMA was similar to that on the HDN of MCHA [4]. As in the HDN of MCHA, the higher selectivity of MCHE and lower selectivity of MCH in the HDN of OMA means that the formation of MCHE from MCHA was promoted, while its further

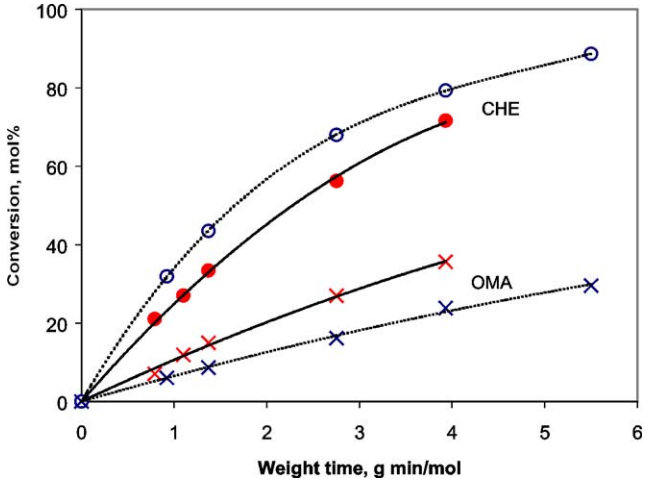

Fig. 5. Effect of support on the HDN of 7 kPa OMA and the hydrogenation of 4 kPa CHE at 370 °C over NiMo/Al_2O_3 (dashed lines) and NiMo/ASA (solid lines).

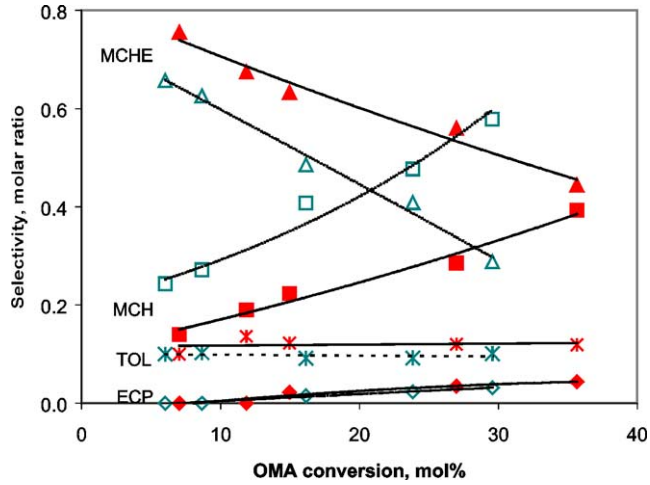

Fig. 6. Effect of support on the selectivity to MCHE (▲), MCH (■), TOL (∗), and ECP (◆) during the HDN of 7 kPa OMA at 370 °C over NiMo/Al_2O_3 (dashed lines) and NiMo/ASA (solid lines).

hydrogenation to MCH was inhibited by the presence of the nitrogen-containing compounds. This trend is more obvious for the NiMo/ASA than for the NiMo/Al_2O_3 catalysts. The selectivity of ECP and toluene was hardly influenced by the support. We have noticed that the ASA-supported catalyst has a larger surface area than the Al_2O_3-supported catalyst. A higher dispersion of NiMoS might thus be expected. However, characterization results showed that owing to a weaker interaction among Ni, Mo, and the ASA support, a lower dispersion and higher stacking of MoS_2 was obtained. The Ni and Mo species tend to adsorb preferentially on the alumina sites of the ASA support [37].

3.3. Fluorination effect

After fluorination, the HDN conversion of OMA increased by a factor of 2 over both catalysts, while the conversion of CHE hydrogenation hardly changed for the Al_2O_3-supported catalyst and slightly increased for the ASA-supported catalyst (Figs. 7a and 7b). This indicates that the hydrogenation of CHE occurs on a different kind of site as the HDN of OMA. The slight increase of the hydrogenation of CHE cannot be attributed to the direct effect of fluorination, because fluorination has no influence on olefin hydrogenation [5]. The effect observed in the present case must be due to the faster HDN reaction, which diminishes the inhibition of OMA (and the possibly formed MCHA) on the hydrogenation (cf. Fig. 3). The higher HDN activity might be attributed to a higher stacking of the MoS_2 after fluorination, which enhances the saturation of aromatic rings [34,35,38,39], and in turn enhances the HDN of aromatic nitrogen-containing compounds. The effect of fluorination was much stronger on the HDN of OMA than on the HDN of MCHA [4]. This indicates that the rate-determining step in the HDN of OMA, the hydrogenation of the phenyl ring of OMA, is strongly promoted by the fluorination. The selectivity for MCHE was increased sub-

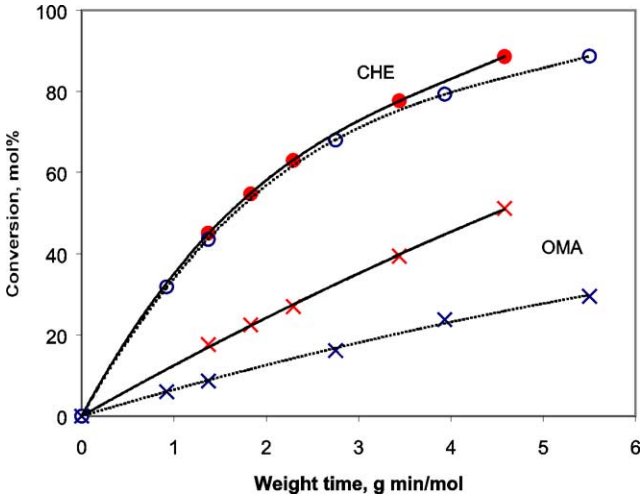

(a)

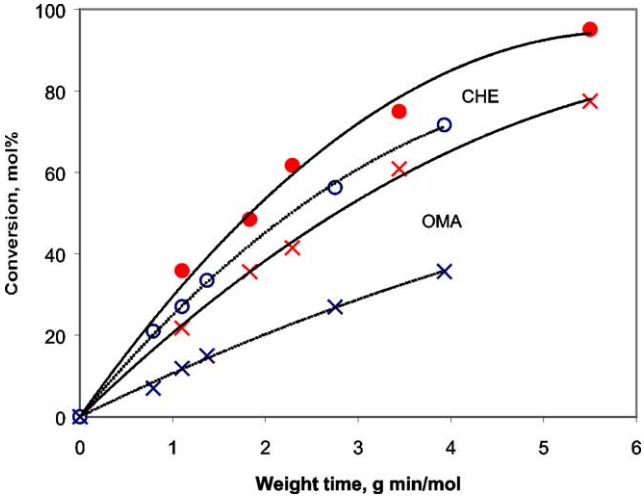

(b)

Fig. 7. Effect of fluorination on the HDN of 7 kPa OMA and the hydrogenation of 4 kPa CHE at 370 °C over (a) $NiMo/Al_2O_3$ and (b) NiMo/ASA (dashed lines for fluorine-free catalyst and solid lines for fluorinated catalyst).

stantially with the fluorinated catalyst in the HDN of OMA, while the MCH selectivity decreased (Fig. 8). This is caused by the strong inhibition of OMA (and MCHA) as well. Fluorination promotes the formation of MCHE, but not its further hydrogenation, and thus leads to an increased accumulation of MCHE. The selectivities for toluene and ECP did not depend on the presence of fluorine. The toluene selectivity was independent of the OMA conversion. The effect of water formed during sulfidation (fluorination) might be a possible driving force for the redispersion (higher stacking) of MoS_2 on ASA supports. However, we believe that the catalyst (50 mg) was already highly (at least 95%) sulfided after a long sulfidation process and maintaining 2 h at 370 °C, especially for the ASA-supported catalyst in which the Ni and Mo interact much weaker with the support. Thus, the additional 48 h do not form much water during the in situ fluorination. Furthermore, in a study of a WS_2-based cata-

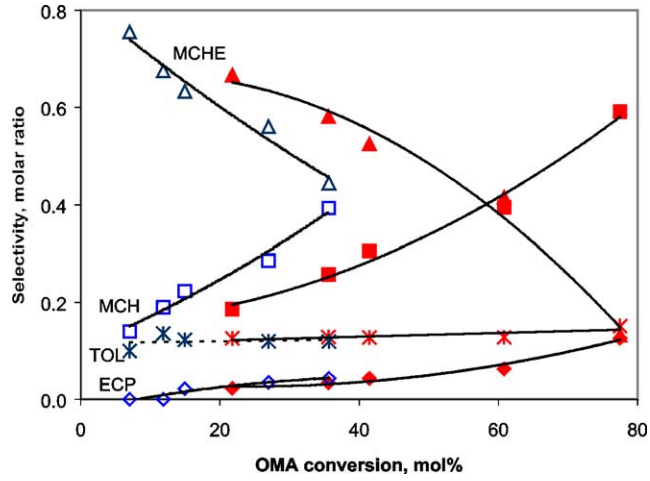

Fig. 8. Effect of fluorination on the selectivity to MCHE (▲), MCH (■), TOL (∗), and ECP (◆) during the HDN of 7 kPa OMA at 370 °C over fluorine-free NiMo/ASA (dashed lines) and fluorinated NiMo/ASA (solid lines).

lyst prepared by ammonium tetrathiotungstate, in which all the tungsten is already in the sulfidic form, the addition of fluorine still caused a higher stacking of WS_2 [40]. Therefore, we exclude this possibility.

3.4. HDN kinetics of OMA

Kinetic modeling was based on the reaction scheme shown in Fig. 1. Since MCHA was not detected when OMA was used as the reactant, we could not model the HDN of OMA with a reaction network including MCHA. Therefore, we assumed in the kinetic treatment that a direct pathway for the reactions from OMA to MCHE and MCH existed. Furthermore, we are mainly interested in HDN in this work, not in the hydrogenation of MCHE to MCH. Therefore we classify the reactions in two categories: first hydrogenation to MCHA followed by the formation of MCHE and MCH (noted as MC), and second the direct hydrogenolysis to toluene (noted as TOL). The small amount of ECP formed was included in MC. These two reactions take place on the same kind of sites, thus we have the following Langmuir–Hinshelwood equations:

$$\frac{dP_{MC}}{d\tau} = \frac{k_1 K_{OMA} P_{OMA}}{1 + K_{OMA} P_{OMA}}, \tag{1}$$

$$\frac{dP_{TOL}}{d\tau} = \frac{k_2 K_{OMA} P_{OMA}}{1 + K_{OMA} P_{OMA}}, \quad \text{and} \tag{2}$$

$$-\frac{dP_{OMA}}{d\tau} = \frac{dP_{MC}}{d\tau} + \frac{dP_{TOL}}{d\tau},$$

where k_1 and k_2 are the reaction rate constants for the formation of MC (MC = MCHE + MCH + ECP) and TOL, respectively. K_{OMA} is the adsorption constant of OMA on the HDN sites. The adsorption constants of MCHE, MCH, ECP, and TOL were neglected because of the much stronger adsorption of OMA [3–5]. The adsorption of NH_3 is also

Table 1
Fitted parameters for the HDN of OMA on $NiMo/Al_2O_3$

Catalyst	k_1 (kPa mol g^{-1} min^{-1})	k_2 (kPa mol g^{-1} min^{-1})	K_{OMA} (kPa^{-1})	MSC
$NiMo/Al_2O_3$				
330 °C	0.13 (0.006)	0.011 (0.003)	0.58 (0.13)	7.7
350 °C	0.27 (0.003)	0.023 (0.002)	0.47 (0.05)	9.0
370 °C	0.52 (0.004)	0.052 (0.004)	0.37 (0.03)	8.7
F-$NiMo/Al_2O_3$				
330 °C	0.25 (0.002)	0.025 (0.002)	0.60 (0.06)	8.9
350 °C	0.56 (0.014)	0.061 (0.006)	0.46 (0.05)	6.7
370 °C	1.14 (0.009)	0.154 (0.009)	0.36 (0.03)	6.4

very weak on these sites and was neglected [3,41]. P_i is the partial pressure of the components in the reactor.

All reactions were performed at a total pressure of 5.0 MPa and a partial pressure of hydrogen at the reactor inlet of 4.8 MPa. The kinetic data were obtained after 20 h on stream when the catalyst was stabilized at 370 °C. No deactivation was observed during the experiments. Four initial partial pressures of OMA were used at each temperature, and at each OMA initial partial pressure more than five weight times were measured. The temperatures studied were 330, 350, and 370 °C. Kinetic modeling was performed with the program SCIENTIST based on the kinetic data obtained at these five weight times, four OMA initial partial pressures, and three temperatures. The resulting reaction rate constants and adsorption constants for the different reaction steps are shown in Tables 1 and 2 (with standard deviation in parentheses). The goodness-of-fit is indicated by the model selection criterion (MSC) and is defined by the formula:

$$\mathrm{MSC} = \ln\left(\frac{\sum_{i=1}^{n} w_i (Y_{\mathrm{obs}_i} - \overline{Y}_{\mathrm{obs}})^2}{\sum_{i=1}^{n} w_i (Y_{\mathrm{obs}_i} - Y_{\mathrm{cal}_i})^2}\right) - \frac{2p}{n},$$

where $\overline{Y}_{\mathrm{obs}}$ is the weighted mean of the observed data Y_{obs_i}, Y_{cal_i} are the calculated data, p and n are the number of parameters and the measured points in the model, respectively, and w_i are the weights applied to the points. All the weight factors were taken to be equal to 1 in our fitting. The larger the value of MSC, the better the fit. As an illustration of the fittings, the experimental results obtained at 370 °C are compared with fits based on Eqs. (1) and (2) in Fig. 9.

Table 2
Fitted parameters for the HDN of OMA on NiMo/ASA

Catalyst	k_1 (kPa mol g^{-1} min^{-1})	k_2 (kPa mol g^{-1} min^{-1})	K_{OMA} (kPa^{-1})	MSC
NiMo/ASA				
330 °C	0.17 (0.003)	0.018 (0.003)	1.03 (0.10)	8.1
350 °C	0.35 (0.004)	0.036 (0.004)	0.75 (0.12)	8.3
370 °C	0.69 (0.008)	0.093 (0.008)	0.60 (0.11)	7.2
F-NiMo/ASA				
330 °C	0.39 (0.007)	0.042 (0.007)	0.38 (0.05)	7.0
350 °C	0.97 (0.010)	0.110 (0.010)	0.30 (0.03)	6.5
370 °C	2.11 (0.017)	0.300 (0.015)	0.21 (0.02)	6.3

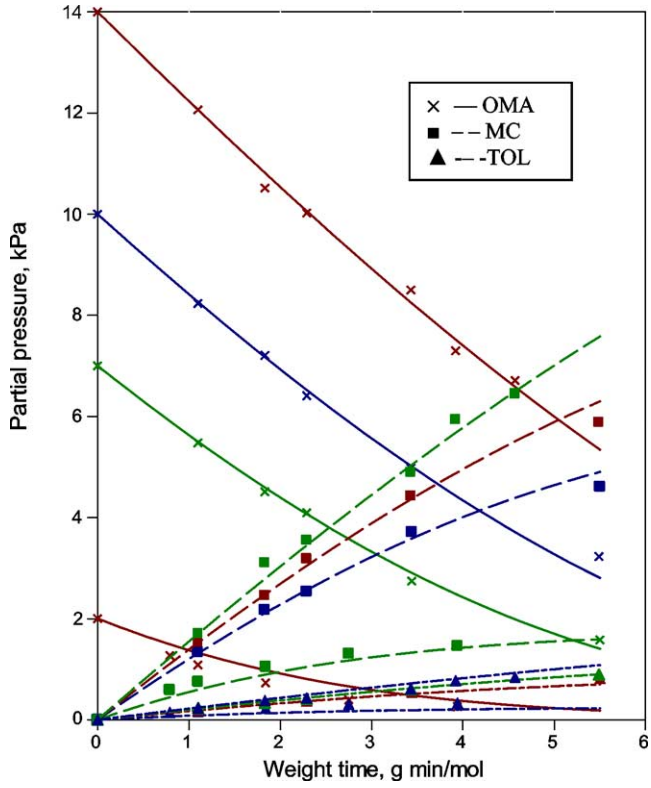

Fig. 9. An illustration of the fit for the HDN of OMA over F-NiMo/ASA at 370 °C (lines are the fitted results and points are the experimental data).

Over the Al_2O_3-supported catalyst (Table 1), the HDN reaction rate constants for path 1 increased by a factor of about 2 after fluorination at all three temperatures studied, while those for path 2 showed an even greater promotion. However, hydrogenolysis only contributes about 10% to the total conversion. The adsorption equilibrium constant of OMA on the HDN sites did not change by fluorination.

For the ASA-supported catalyst (Table 2), the HDN rate constant increased 2.5 to 3 times for both reaction pathways after fluorination. The adsorption constant of OMA on the HDN sites is somewhat higher on the ASA-supported catalyst than on its Al_2O_3-supported counterpart. After fluorination the adsorption equilibrium constant decreased.

From the results obtained at different temperatures, the activation energies of the HDN reaction paths were calculated from the Arrhenius plot of $\ln k$ versus $1/T$ (Fig. 10 and Table 3). There seems to be a slight increase of the activation energies with fluorination and with going from Al_2O_3-supported to ASA-supported NiMo. However, these differences are insignificant within the uncertainties of the measurements. The preexponential factors increase by two order of magnitudes with fluorination. This indicates that only the number of the catalytic sites increased by fluorination, while the intrinsic activity of the sites remained unchanged. Since we did not fix the activation energies in our fitting, a compensation effect may exist in the system. Therefore, the two orders of magnitude difference in the

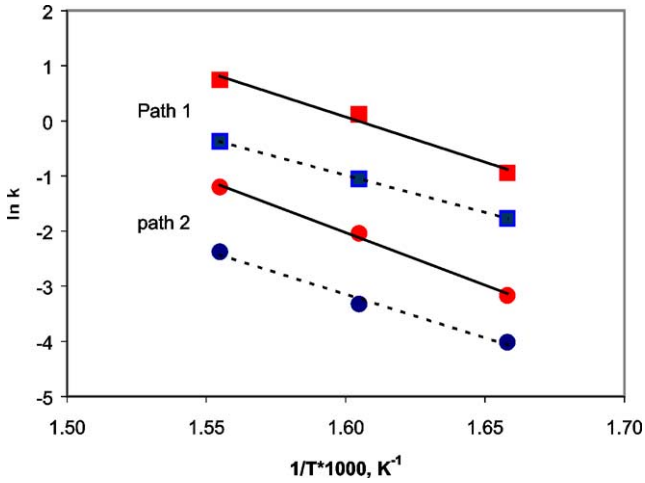

Fig. 10. $\ln k$ versus $1/T$ plot for the HDN of OMA over NiMo/ASA (dashed lines for fluorine-free catalyst and solid lines for fluorinated catalyst).

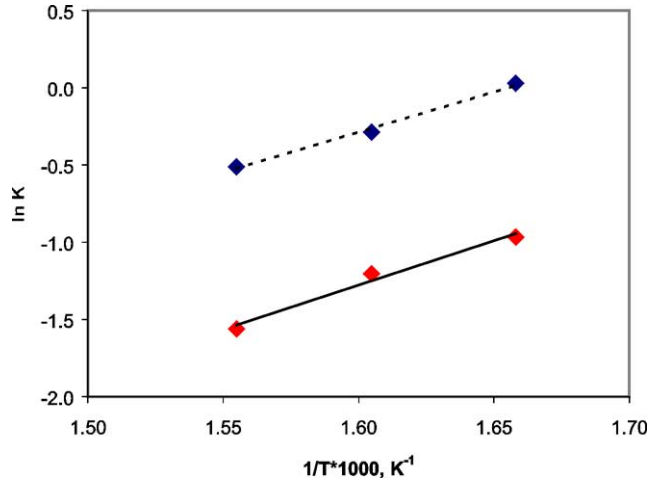

Fig. 11. $\ln K$ versus $1/T$ plot for the HDN of OMA over NiMo/ASA (dashed lines for fluorine-free catalyst and solid lines for fluorinated catalyst).

Table 3
Activation energies and heats of adsorption for the HDN of OMA

	NiMo/Al_2O_3	F-NiMo/Al_2O_3	NiMo/ASA	F-NiMo/ASA
E (kJ mol^{-1})				
Path 1	112 (9)	122 (14)	113 (16)	136 (8)
Path 2	125 (25)	144 (16)	132 (18)	159 (25)
A (kPa mol g^{-1} min^{-1})				
Path 1	6×10^8	1×10^{10}	1×10^9	3×10^{11}
Path 2	7×10^8	8×10^{10}	5×10^9	2×10^{12}
$-\Delta H_{ads}$ (kJ mol^{-1})	36 (7)	41 (5)	44 (7)	48 (6)
K_0 (kPa^{-1})	4×10^{-4}	2×10^{-4}	2×10^{-4}	3×10^{-5}

preexponential factors do not mean that the reaction rates should be two orders of magnitude faster.

Like the activation energies, the heats of adsorption can be obtained from the Arrhenius plot of $\ln K$ versus $1/T$ (Fig. 11 and Table 3). The heat of adsorption of OMA on the catalytic sites for HDN showed no substantial difference between the fluorine-free catalysts and their fluorinated counterparts. This further confirms that fluorination mainly increases the number of active sites for HDN without altering the nature of the sites.

The fact that hardly any MCHA is observed in the HDN of OMA suggests that the rate of reaction of MCHA is very much faster than its rate of formation. From the present results on the HDN of OMA and those obtained earlier on the HDN of MCHA [4], the ratios of the apparent rate constants $k' = kK/(1 + KP)$ for the HDN of 14 kPa OMA and for the HDN of 14 kPa MCHA to MCHE and MCH can be obtained. As Table 4 shows, the ratios of k'_{MCHA}/k'_{OMA} range from 4.5 to 7.7 at 330 °C and from 5.3 to 12 at 350 °C. This indicates that the apparent rate constants do not differ enough to explain why no MCHA was observed in the HDN of OMA. For instance, considering the consecutive reaction

$$\mathrm{OMA} \overset{k'_{OMA}}{\rightarrow} \mathrm{MCHA} \overset{k'_{MCHA}}{\rightarrow} \mathrm{MCHE} + \mathrm{MCH}$$

Table 4
Values of k'_{MCHA}/k'_{OMA}

	NiMo/Al_2O_3	F-NiMo/Al_2O_3	NiMo/ASA	F-NiMo/ASA
330 °C	7.7	5.2	7.2	4.5
350 °C	12	6.4	10	5.3

and assuming pseudo first-order reactions, the maximum concentration of MCHA is

$$(\mathrm{MCHA/OMA_0})_{max} = (k'_{OMA}/k'_{MCHA})^{k'_{MCHA}/(k'_{MCHA}-k'_{OMA})}$$

and the weight time for the maximum MCHA concentration is

$$\tau_{max} = \ln(k'_{OMA}/k'_{MCHA})/(k'_{OMA} - k'_{MCHA}).$$

At 330 and 350 °C, the maximum MCHA concentration should then be between 7 and 14 mol% of the initial OMA concentration, and the weight time for the maximum MCHA concentration should be between 1.3 and 2.6 min g mol^{-1} at 330 °C, and below 1 min g mol^{-1} at 350 °C for all catalysts. With a detection limit of at least 0.5 mol%, we should have been able to detect these amounts of MCHA under our reaction conditions ($\tau \geqslant 0.5$ min g mol^{-1}). Therefore, there must be other factors why we did not detect MCHA formed in the pores of the catalysts.

A reason for the discrepancy between the ratio of the rate constants and the very low concentration of MCHA observed might be "hidden kinetics." If during the HDN of OMA the reaction of MCHA at the catalyst surface is much faster than MCHA desorption, then equilibrium between MCHA at the catalyst surface and in the gas phase is not established. In that case, the expected partial pressure of MCHA cannot be estimated from a Langmuir–Hinshelwood equation. It is conceivable that this equilibrium is attained in the HDN reaction of MCHA itself, but not in that of OMA. During the HDN of MCHA, the basic MCHA molecule will adsorb in σ mode with its free electron pair toward the

surface. This configuration is not well suited for Hofmann elimination of the H atoms at the β carbon atom, which in this σ bonding configuration point away from the catalyst surface. On the other hand, during the HDN of OMA, the lone pair in OMA is conjugated with the aromatic ring and as a consequence, OMA is less basic as MCHA and can adsorb in π mode on the metal sulfide surface. In this configuration, parallel to the surface, it cannot only easily be hydrogenated to MCHA, but the resulting MCHA can easily undergo β-H elimination before its desorption to the gas phase. This would explain why a measurement starting with MCHA comes up with a lower reaction rate for MCHA than that of a measurement starting with OMA.

4. Conclusions

Different pathways are involved in the HDN of OMA. The direct hydrogenolysis of the C(sp^2)–N bond accounts for 10% of the whole conversion, while the path via hydrogenation to MCHA, followed by NH_3 elimination, is the main HDN reaction mechanism.

The ASA-supported catalysts show a higher HDN activity of OMA than their Al_2O_3-supported counterparts. A much more pronounced HDN performance for the in situ fluorinated catalysts was observed for the HDN of OMA than for MCHA. This is caused by the higher activity for the hydrogenation of the aromatic ring involved in the HDN of OMA, induced by the higher stacking of MoS_2 in the ASA-supported catalysts.

Fluorination enhances the HDN activities of both the Al_2O_3- and the ASA-supported catalysts. Kinetic parameters indicate that the intrinsic activity of the active sites is not influenced; only the number of the HDN sites is increased.

References

[1] R. Prins, in: G. Ertl, H. Knözinger, J. Weitkamp (Eds.), Handbook of Heterogeneous Catalysis, Vol. 4, VCH, Berlin, 1997, p. 1908.
[2] F. Rota, R. Prins, Stud. Surf. Sci. Catal. 127 (1999) 319.
[3] F. Rota, R. Prins, Topics Catal. 11/12 (2000) 327.
[4] L. Qu, R. Prins, J. Catal. 210 (2002) 183.
[5] L. Qu, R. Prins, J. Catal. 207 (2002) 286.
[6] J. Ramirez, R. Cuevas, A. Lopez Agudo, S. Mendioroz, J.L.G. Fierro, Appl. Catal. 57 (1990) 223.
[7] A. Benitez, J. Ramirez, A. Vazquez, D. Acosta, A. Lopez Agudo, Appl. Catal. A 133 (1995) 103.
[8] A. Benitez, J. Ramirez, J.L.G. Fierro, A. Lopez Agudo, J. Catal. 144 (1996) 343.
[9] A. Benitez, J. Ramirez, J. Cruz-Reyes, A. Lopez Agudo, J. Catal. 172 (1997) 137.
[10] J.A.R. Van Veen, H.A. Colijn, P.A.J.M. Hendriks, A.J. van Welsenes, Fuel Process. Techn. 35 (1993) 137.
[11] L. Qu, M. Jian, Y. Shi, D. Li, Chin. J. Catal. 19 (1998) 608.
[12] J.L.G. Fierro, R. Cuevas, J. Ramirez, A. Lopez Agudo, Bull. Soc. Chim. Belg. 100 (1991) 945.
[13] M. Lewandowski, Z. Sarbak, Appl. Catal. A 156 (1997) 181.
[14] C. Kwak, M.Y. Kim, C.J. Song, S.H. Moon, Stud. Surf. Sci. Catal. 121 (1998) 283.
[15] C. Kwak, S.H. Moon, Korean J. Chem. Eng. 16 (1999) 608.
[16] H.K. Matralis, A. Lycourghiotis, P. Grange, B. Delmon, Appl. Catal. 38 (1988) 273.
[17] H.K. Matralis, Ch. Papadopoulou, A. Lycourghiotis, Appl. Catal. 116 (1994) 273.
[18] K. Jiratova, M. Kraus, Appl. Catal. 27 (1986) 21.
[19] A.N. Startsev, O.V. Klimov, A.V. Kalinin, V.M. Mastikhin, Kinet. Catal. 35 (1994) 601.
[20] J. Ramirez, R. Cuevas, L. Gasque, M. Vrinat, M. Breysse, Appl. Catal. 71 (1991) 351.
[21] P. Ladeur, B. Post, M. Fagot, J.P. Saint (Shell International Research B.V.), UK Patent 2,024,642, 1979.
[22] R.J. Bertolacini, J.F. Mosby, J.G. Schwartz (Standard Oil Company), US Patent 4,420,388, 1983.
[23] T. Fujikawa, K. Idei, T. Ebihara, H. Mizuguchi, K. Usui, Appl. Catal. A 192 (2000) 253.
[24] V.L. Barrio Cagigal, P.L. Arias Ergueta, J.F. Cambra Ibanez, M.B. Guemez Bilbao, B. Pawelec, J.L. Garcia Fierro, Abstracts of Papers (PETR-043), 223rd ACS National Meeting, Orlando, FL, April 7–11, 2002.
[25] M. Vaarkamp (Engelhard Co.), Eur. Patent 1,147,811 A1, 2001.
[26] J.W. Ward (Union Oil Co.), CA, Eur. Patent 325,827 A2, 1989.
[27] C.M. Van Ballegoy, J.T. Daamen, J.-P. Gilson, A.H. Klazinga, A. Hoek (Shell Internationale Research Maatschappij B.V.), Eur. Patent 532,118 A1, 1992.
[28] J.W. Gosselink, L.R. Groeneveld, H. Schaper, J.A.R. van Veen (Shell Internationale Research Maatschappij B.V.), Eur. Patent 428,224 A1, 1991.
[29] E. Benazzi, S. Kasztelan (Institut Français du Petrole, France), DE 10,007,889 A1, 2000.
[30] R. Navarro, B. Pawelec, J.L.G. Fierro, P.T. Vasudevan, Appl. Catal. A 148 (1996) 23.
[31] L.A. Gerritsen, S.L. Lee (Akzo Nobel N.V.), Eur. Patent 870,817 A1, 1998.
[32] R. Cowan, M. Hoglin, H. Reinink, J. Ysaebaert, D. Chadwick, Catal. Today 45 (1998) 381.
[33] T.I. Koranyi, M. Dobrovolszky, T. Koltai, K. Matusek, Z. Paal, P. Tetenyi, Fuel Process. Techn. 61 (1999) 55.
[34] W.R.A.M. Robinson, J.A.R. van Veen, V.H.J. de Beer, R.A. van Santen, Fuel Process. Techn. 61 (1999) 89.
[35] W.R.A.M. Robinson, J.A.R. van Veen, V.H.J. de Beer, R.A. van Santen, Fuel Process. Techn. 61 (1999) 103.
[36] E. Peeters, C. Geantet, J.L. Zotin, M. Breysse, M. Vrinat, Stud. Surf. Sci. Catal. 130C (2000) 2837.
[37] L. Qu, W. Zhang, P.J. Kooyman, R. Prins, J. Catal., in press.
[38] M. Daage, R. Chianelli, J. Catal. 149 (1994) 414.
[39] E.J.M. Hensen, P.J. Kooyman, Y. van der Meer, A.M. van der Kraan, V.H.J. de Beer, J.A.R. van Veen, R.A. van Santen, J. Catal. 199 (2001) 224.
[40] M. Sun, P.J. Kooyman, R. Prins, J. Catal. 206 (2002) 368.
[41] C.N. Satterfield, S.H. Yang, Ind. Eng. Chem. Process. Des. Dev. 23 (1984) 11.